Frustrated incomplete donor ionization in ultra-low resistivity germanium films

Chi Xu, C. L. Senaratne, J. Kouvetakis, and J. Menéndez

Citation: Applied Physics Letters **105**, 232103 (2014); doi: 10.1063/1.4903492
View online: http://dx.doi.org/10.1063/1.4903492
View Table of Contents: http://scitation.aip.org/content/aip/journal/apl/105/23?ver=pdfcov
Published by the AIP Publishing

Frustrated incomplete donor ionization in ultra-low resistivity germanium films

Chi Xu,[1] C. L. Senaratne,[2] J. Kouvetakis,[2] and J. Menéndez[1]
[1]*Department of Physics, Arizona State University, Tempe, Arizona 85287-1504, USA*
[2]*Department of Chemistry and Biochemistry, Arizona State University, Tempe, Arizona 85287-1604, USA*

(Received 15 October 2014; accepted 22 November 2014; published online 8 December 2014)

The relationship between carrier concentration and donor atomic concentration has been determined in *n*-type Ge films doped with P. The samples were carefully engineered to minimize non-active dopant incorporation by using specially designed $P(SiH_3)_3$ and $P(GeH_3)_3$ hydride precursors. The *in situ* nature of the doping and the growth at low temperatures, facilitated by the Ge_3H_8 and Ge_4H_{10} Ge sources, promote the creation of ultra-low resistivity films with flat doping profiles that help reduce the errors in the concentration measurements. The results show that Ge deviates strongly from the incomplete ionization expected when the donor atomic concentration exceeds $N_d = 10^{17}\,cm^{-3}$, at which the energy separation between the donor and Fermi levels ceases to be much larger than the thermal energy. Instead, essentially full ionization is seen even at the highest doping levels beyond the solubility limit of P in Ge. The results can be explained using a model developed for silicon by Altermatt and coworkers, provided the relevant model parameter is properly scaled. The findings confirm that donor solubility and/or defect formation, not incomplete ionization, are the major factors limiting the achievement of very high carrier concentrations in *n*-type Ge. The commercially viable chemistry approach applied here enables fabrication of supersaturated and fully ionized prototypes with potential for broad applications in group-IV semiconductor technologies. © *2014 AIP Publishing LLC*. [http://dx.doi.org/10.1063/1.4903492]

The development of germanium-based *n*-FETs requires the fabrication of ultra-highly doped layers with carrier concentrations preferably exceeding $5 \times 10^{19}\,cm^{-3}$ (Ref. 1). To achieve this goal, donor implantation has been pursued by several groups,[2–8] while other authors emphasize the advantages of *in-situ* doping.[9–19] Regardless of the specific approach, the implicit assumption underlying this quest is that germanium deviates strongly from the incomplete donor ionization predicted when the doping level is so high that $E_d - \mu \gg k_B T$ is no longer valid (Here, E_d is the donor energy level, μ the Fermi level, k_B Boltzmann's constant, and T the absolute temperature). Otherwise, a carrier concentration of $5 \times 10^{19}\,cm^{-3}$ at room temperature would be unattainable, since it would require an atomic donor concentration of $2 \times 10^{21}\,cm^{-3}$, well beyond the solubility limit of any dopant in Ge.[1] Carrier concentrations above the predictions from the standard theory are in fact well known in the case of Si, and have been explained in terms of dopant-induced modifications in the density of states. Altermatt and co-workers have developed an explicit model of the density of states that accounts for many electrical and optical properties of highly doped Si.[20] The model contains several parameters, but only one of them—the fraction b of donor electrons bound to isolated donor clusters—plays a key role in determining the degree of incomplete ionization.[21] For $b = 1$, the nature of the donor states is unchanged by doping and incomplete ionization is expected to occur as predicted by the standard theory. For $b < 1$, a fraction of $(1–b)$ of the donor electrons is in the conduction band and contributes to the electrical conductivity regardless of temperature, thereby leading to carrier concentrations well above those predicted from the standard theory with $b = 1$. The situation is much less clear in the case of germanium. The classic work of Fistul *et al.* (Ref. 22) exploring the solubility of electrically active phosphorus in Ge could be interpreted in terms of standard incomplete ionization with $b = 1$. More recently, Koike *et al.* (Ref. 23) carried out a detailed study of dopant activation in ion-implanted Ge layers and found that their results were consistent with $b = 1$. The authors suggest that the presence of dopant-vacancy pairs and/or clustering of impurities hinder the formation of an impurity band. In this letter, we present a study of P-doped Ge layers grown on Ge-buffered Si substrates. Our results show clear evidence for $b < 1$ at high carrier concentrations, as seen in silicon. Moreover, the observed carrier concentrations as a function of the atomic doping concentrations are in very good agreement with the predictions from the Altermatt model using a b parameter scaled from Si to Ge.

The fundamental challenge of an incomplete ionization study is that the amount of inactive donors must be minimized. Otherwise, the observation of carrier concentrations smaller than atomic dopant concentrations could be mistakenly viewed as evidence for incomplete ionization, when, in fact, they may arise in a full-ionization context if only a fraction of the dopants are in inactive sites. Our basic strategy to minimize inactive P is the use of $P(MH_3)_3$ (M = Si, Ge) as the source of phosphorus. The fact that P is already bonded to three Ge or Si atoms in these compounds is expected to promote its substitutional incorporation into the diamond lattice and reduce donor clustering. Successful doping of Ge-like materials with $P(GeH_3)_3$ has been demonstrated using the commercially available Ge_2H_6 or Ge_3H_8 precursors as the source of Ge atoms.[24–29] The use of $P(SiH_3)_3$ as a pure-Ge dopant had not been previously reported.

Two screening criteria were used to deselect samples that might contain substantial amounts of inactive P. The

first criterion is that the resistivity of the doped layers should not be much higher than reported values of the resistivity of Ge as a function of carrier concentration. The second criterion is based on the observation that whether incomplete ionization takes place or not, carrier concentrations should increase monotonically as a function of atomic donor concentration. Therefore, samples with decreased (well beyond experimental error) carrier concentrations relative to samples with lower (well beyond experimental error) dopant concentrations are not included in the analysis. It turns out that all samples grown with the $P(MH_3)_3$ precursors satisfy the resistivity criterion, whereas a few samples with dopant atomic concentrations in the $\sim 10^{20}\,cm^{-3}$ range deviate from the monotonicity requirement.

The doped layers were grown on Ge-buffered Si substrates either by gas-source molecular epitaxy (GSME) using Ge_4H_{10} as the source of Ge, or by ultra-high vacuum chemical vapor deposition (UHV-CVD) using Ge_3H_8 as the source of Ge. The use of higher-order Ge-hydrides was motivated by the excellent quality of Ge layers grown recently at low temperatures with these compounds.[30] These low growth temperatures preserve the flat doping profiles characteristic of *in situ* doping, thereby reducing the uncertainties in the measurements of carrier and donor concentrations. Undoped buffer Ge layers with thicknesses between 600 nm and 2100 nm were grown by GSME on (001) Si wafers at substrate temperature near 350 °C and pressure of 1.1×10^{-4} Torr using Ge_4H_{10}/H_2 mixtures. For growth of the doped layer on the same reactor, the Ge-buffered samples were subjected to a brief *in situ* annealing step at 650 °C for 3 min. The *n*-type layers, with thicknesses ranging between 180 nm and 430 nm, were then grown at the same temperature as the buffer using gaseous mixtures of H_2, Ge_4H_{10}, and varying amounts of $P(MH_3)_3$. For UHV-CVD growth, the buffer layers were removed from the GSME reactor and cleaved into 45 mm × 45 mm pieces. The samples were then cleaned by dipping into a 5% HF solution prior to being loaded into the growth chamber. After thermal equilibrium was achieved, the growth was carried out at 340 °C and 0.2 Torr by flowing appropriate amounts of $Ge_3H_8/P(MH_3)_3/H_2$ gas mixtures into the chamber. Thicknesses ranged from 135 nm to 255 nm.

The structural properties of the samples were characterized by Rutherford backscattering (RBS), high-resolution X-ray diffraction (HRXRD), cross-sectional transmission electron microscopy (XTEM), and atomic force microscopy (AFM). The AFM study reveals flat surfaces with RMS roughness of less than 1 nm, indicating layer-by-layer growth in spite of the interruption after the buffer growth. XRD 224 reciprocal space maps (RSMs) signal the presence of residual (~0.1%) tensile strains in the Ge buffers as shown in Fig. 1 for a representative sample. The single 224 peak in the figure corresponds to the combined contributions from the *n*-type and undoped layers, indicating that the two materials have the same lattice constant.

Further characterizations by XTEM demonstrate that the films comprise mono-crystalline layers with epitaxial interfaces and flat surfaces. A typical micrograph is shown in Fig. 1, illustrating a few scattered defects in the lower intrinsic region of the device while the upper doped segment is

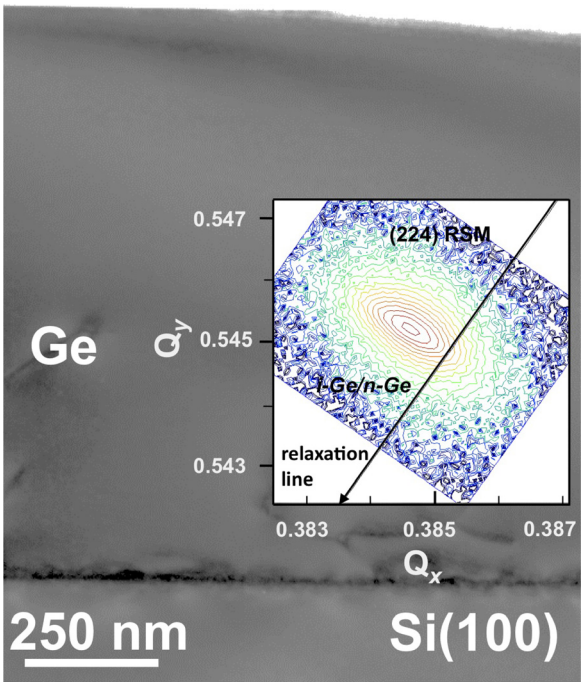

FIG. 1. Structural data for a representative sample comprising an intrinsic Ge buffer and an *n*-type top layer co-doped with P ($9.0 \times 10^{18}\,cm^{-3}$) and Si ($3.1 \times 10^{19}\,cm^{-3}$). The XTEM image shows the entire 1200 nm thickness of the film. The upper n-type portion is flat and defect-free within the field of view. The inset shows a 224 XRD RSM indicating that the layers are pseudomorphic and tensile strained on the Si substrate.

virtually defect-free. The micrograph also reveals uniform phase contrast across the transition region from undoped to doped sections, indicating that the growth is continuous.

Critical for the purpose of this study is the independent determination of the atomic phosphorus concentration N_d and the free carrier concentration n in the conduction band. We use Secondary Ion Mass Spectrometry (SIMS) for the former and infrared spectroscopic ellipsometry (IRSE) for the latter. The SIMS data were calibrated using a reference standard. Figure 2(a) shows typical SIMS plots. The flatness of the as-grown doping profile makes it possible to obtain N_d

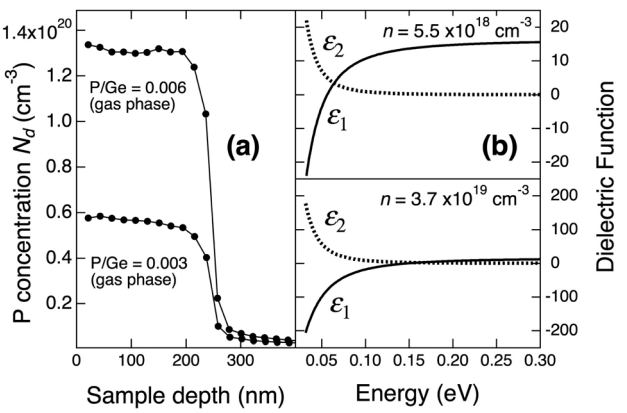

FIG. 2. (a) SIMS depth profiles for selected P-doped samples. Notice the profile flatness, even when plotted on a linear scale. The film P atomic concentrations scale with the ratio of P and Ge atoms in the precursor gases. (b) Dielectric function of two P-doped Ge films obtained from IRSE measurements. The real and imaginary parts show the characteristic energy dependence associated with the Drude conductivity. The functional dependences are similar at low- and high-doping levels, but the dielectric function magnitudes are drastically different.

with errors typically less than 5%. Such flatness would be nearly impossible to achieve with implanted samples, which therefore are not optimal for this type of studies. Although not shown in Fig. 2, the SIMS data also confirm the presence of Si when using the $P(SiH_3)_3$ precursor. The Si/P ratio in the films is at or above the 3:1 precursor ratio in samples grown by GSME, and below 3:1 when the growth technique is UHV-CVD. A full account of this intriguing behavior will be published elsewhere.

IRSE is the most straightforward method for the determination of n because it is a contactless technique which, to an excellent approximation, does not require any knowledge of the transport properties of the doped material.[31,32] Our measurements were carried out at room temperature using a variable-angle instrument manufactured by J. A. Woollam Co. We covered the 0.03 eV–0.8 eV spectral range with a resolution of 2 meV. Most samples were measured using a single angle of incidence of 70°. A few samples were measured at three angles of incidence, but the results were virtually unchanged. Figure 2(b) shows examples of the real and imaginary part of the dielectric function. The samples were modeled as a two-layer system (buffer and doped film) on a Si substrate. We also included a 1 nm surface roughness layer consisting of 50% voids/50% doped Ge in the Brugemann approximation. The optical constants of the substrate and buffer layer were determined from earlier measurements on nominally identical samples. The doped layer optical constants were taken as those of the buffer layer plus a Drude-like contribution given by

$$\varepsilon_{\text{Drude}} = \frac{-\hbar^2}{\varepsilon_0 \rho(\tau E^2 + i\hbar E)} = \frac{-\hbar^2 n e^2}{\varepsilon_0 m^*(E^2 + i\hbar E/\tau)}. \quad (1)$$

Here, ε_0 is the vacuum permittivity, e the electron charge, ρ the resistivity, τ the relaxation time, and m^* the conductivity effective mass. The adjustable parameters of the ellipsometry model are therefore the buffer and doped layer thicknesses and the two Drude model parameters. Our fitted layer thicknesses for the buffer and doped layers are in excellent agreement with RBS, SIMS, and XTEM data.

If the effective mass is known, as is the case in Ge, a fit of the infrared dielectric function with the second form of Eq. (1) yields n and τ. Typical accidental errors in n are less than 2%. The needed effective mass is given by $3/m* = (1/m_{||}) + (2/m_{\perp})$, where $m_{||}$ ($m_{\perp}$) is the longitudinal (transverse) mass of the L-valley in Ge. Using cyclotron resonance, Dresselhaus, Kip, and Kittel (DKK) found these masses to be $m_{||} = (1.58 \pm 0.04)\, m$ and $m_{\perp} = (0.082 \pm 0.001)\, m$ (m is the free electron mass) at 4 K.[33] These values were later corroborated by magnetoabsorption[34] and magnetopiezo-transmission.[35] Particularly remarkable is the agreement on $m_{\perp}$ (which by far gives the dominant contribution to m^*) among these three techniques (better than 3%). Recent theoretical studies also give effective mass values in excellent agreement with the experimental findings.[36,37] Using the DKK values, the effective mass is $m^* = (0.120 \pm 0.001)m$. For use in Eq. (1), this value must be corrected for the changes in the band structure as a function of temperature and doping (gap renormalization), as well as for nonparabolicity effects. Our simulations show that these corrections are small (< 5%) and tend to cancel each other, so that we use the low temperature value $m^* = 0.12\, m$ to analyze our results.

A more conventional approach to determine n is via the Hall effect. We have carried out Hall measurements on several samples. If we assume the Hall coefficient to be given by $R_H = 1/ne$, we obtain values of n that are on average 13% higher than those obtained from IRSE. If we modify the Hall expression using the Hall factor from Ref. 38 and take the effective mass anisotropy into account,[39,40] we obtain carrier concentrations that are on average 8% below the IRSE values. We believe that the ellipsometry results are more accurate because the effective masses are far better known than the Hall factors, but the conclusions of this paper are not affected by such small differences in n.

Figure 3(a) shows the measured n vs N_d for the samples that satisfy the monotonicity criterion, and Fig. 3(b) shows the corresponding resistivities as a function of n. We have also added data from the literature[9] that satisfy the monotonicity criterion, including two data points from Sb-doped Ge samples. (Ref. 41). The dotted lines in the figure correspond to the carrier concentration n and the ionization ratio N_d^+/N_d predicted for pure Ge at room temperature from the neutrality condition

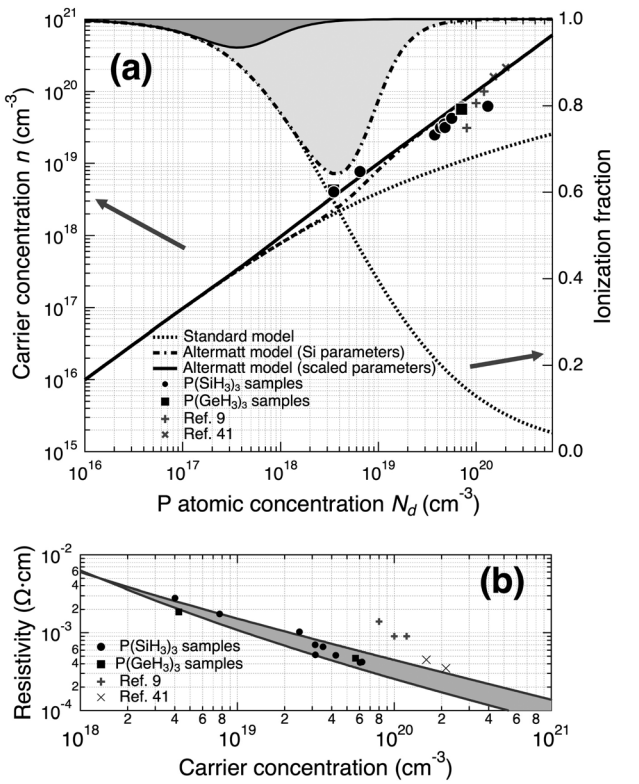

FIG. 3. (a) Experimental carrier concentrations versus atomic donor concentrations (all markers). For the samples grown with the $P(MH_3)_3$ precursors, the error bars are smaller than the symbol size. The dotted lines show the carrier concentration (left axis) and ionization ratio (right axis) predicted from the standard model with $b = 1$. The dash-dotted line is the Altermatt model with the b fraction with Si parameters. The solid line is the Altermatt model with the parameters for b scaled from Si to Ge. (b) Resistivity of the samples as a function of the carrier concentration. The two solid lines show literature values for As-doped Ge (higher resistivity) and Sb-doped Ge (lower resistivity). All samples grown with the $P(MH_3)_3$ precursors have resistivities which within error overlap with the grey area between the two bulk curves.

$$n = N_d^+ + p, \tag{2}$$

where N_d^+ is the ionized donor concentration and p the hole concentration. The calculation was carried out using standard Fermi-Dirac expressions for each of the terms in Eq. (2). For completeness, we included non-parabolicity and band gap renormalization effects, although their effect is minor. Similarly, we find that predictions for $Ge_{1-x}Si_x$ alloys with x as high as $x = 0.1$ are virtually undistinguishable from the dotted lines in Fig. 3(a). Since the highest Si concentration in the samples shown in Fig. 3 is $x = 0.012$ by SIMS, we can safely combine data from samples doped with $P(SiH_3)_3$ or $P(GeH_3)_3$. We see that the standard theory predicts a very significant level of incomplete ionization for $N_d > 5 \times 10^{17}\,cm^{-3}$, but it is apparent that the measured n are well in excess of these theoretical predictions and close to the full ionization limit. Similar observations of frustrated incomplete ionization were made in the case of Si.[20,21] The Si results are described using a model in which only a fraction b of the donor atoms can localize carriers. This is expressed mathematically as

$$N_d^+ = N_d \left[\frac{\frac{1}{2} e^{(E_d-\mu)/k_B T} + 1 - b}{\frac{1}{2} e^{(E_d-\mu)/k_B T} + 1} \right]. \tag{3}$$

Furthermore, the parameter b is well represented with an expression of the form

$$b = \frac{1}{1 + (N_d/N_b)^d}. \tag{4}$$

For P in Si, a good fit of the available experimental data is obtained with $N_b = 6 \times 10^{18}\,cm^{-3}$ and $d = 2.3$ (Refs. 20 and 21). If we recalculate n combining Eqs. (2)–(4) with Si parameters for Eq. (4), we obtain the dash-dotted lines in Fig. 3(a), which are in much better agreement with the experimental data because they indicate essentially full donor ionization beyond $N_d > 2 \times 10^{19}\,cm^{-3}$. Below this range, on the other hand, the theory predicts incomplete donor ionization (below 70% at $N_d = 4 \times 10^{18}\,cm^{-3}$), whereas our data indicate full ionization in this range. We notice, however, that since the Mott transition in Ge occurs at $N_d = 2.6 \times 10^{17}\,cm^{-3}$, as opposed to $3.5 \times 10^{18}\,cm^{-3}$ in Si, the parameter N_b should be proportionally smaller in Ge. If we then use Eq. (4) with $N_b = 4.5 \times 10^{17}\,cm^{-3}$ and $d = 2.3$, we obtain the solid lines in Fig. 3(a), which improve the agreement with the experimental data, particularly in the $10^{18}\,cm^{-3}$ range. Still, the observed n for the $N_d > 2 \times 10^{19}\,cm^{-3}$ samples are somewhat below the predicted full ionization in this range. While this could be partially due to residual systematic errors in our measurements of n and N_d, we believe that—at least, in some cases—the discrepancy is due to the presence of non-activated P in spite of the precautions taken to minimize this effect. This evidence arises from ellipsometric studies of annealed samples, from which we can deduce an increase in the total amount (not n) of free carriers. If we assume the validity of the theoretical prediction of full ionization in this range, these excess carriers must originate from P atoms that were inactive in the as-grown samples. We can then compute the amount of as-grown active P atoms, and when we do so, the points in the figure are displaced to the left and end up even closer to the prediction line, providing a self-consistent confirmation of the theoretical model.

The resistivity values shown in Fig. 3(b) for samples grown with the $P(MH_3)_3$ precursors were obtained from the ellipsometry fits. We have also carried out standard four-probe measurements in selected samples, and we find that the values obtained from such measurements, assuming insulating buffer layers, are about 20% lower. The solid lines in the figure represent fits to the resistivities of As-doped bulk Ge (Ref. 39) and Sb-doped bulk Ge (Ref. 42). We find that our $P(MH_3)_3$-doped Ge-films have resistivities consistent with the bulk measurements. On the other hand, the data from Ref. 9 indicate resistivities that are considerably above the bulk Ge curves, even though their carrier concentrations are consistent with those measured in $P(MH_3)_3$-doped Ge-films. This suggests that the resistivity criterion is a poor predictor of dopant activation. Therefore, donor activation studies based on sheet resistance measurements or spreading resistance profiling may be affected by large errors.

In conclusion, we have shown that the frustration of incomplete ionization observed in Si is also present in Ge. The model built by Altermatt to explain the transport and optical properties of highly doped Si appears to be transferable to Ge, following a natural parameter scaling that provides strong support for the underlying physics in the model. A significant prediction from the scaled model parameters is that incomplete ionization is virtually unobservable in Ge at room temperature (the lowest predicted ionization level is about 90% at $N_d = 3$–$4 \times 10^{17}\,cm^{-3}$, as seen in Fig. 3(a)), whereas the effect is much larger in Si. From a technological perspective, our results indicate that donors in ultrahighly doped Ge with $N_d > 10^{19}\,cm^{-3}$ are essentially fully ionized, so that the donor solubility limit is also the ultimate limit to the carrier concentration that can be achieved. However, if metastable conditions can be achieved that lead to concentrations above the solubility limit, the corresponding carrier concentrations could also become higher if the formation of non-active dopant clusters or defects can be avoided. The doping approach described here appears promising for achieving this requirement.

This work was supported by the Air Force Office of Scientific Research under Contract Nos. DOD AFOSR FA9550-12-1-0208 and DOD AFOSR FA9550-13-1-0022. We are grateful to Dr. Liying Jiang for assistance with TEM characterization and to Dr. Lynda Williams and the NSF-supported ASU SIMS Facility for their support and advice on the critical SIMS measurements.

[1]J. Vanhellemont and E. Simoen, Mater. Sci. Semicond. Process. **15**(6), 642 (2012).
[2]C. O. Chui, K. Gopalakrishnan, P. B. Griffin, J. D. Plummer, and K. C. Saraswat, Appl. Phys. Lett. **83**(16), 3275 (2003).
[3]C. O. Chui, L. Kulig, J. Moran, W. Tsai, and K. C. Saraswat, Appl. Phys. Lett. **87**(9), 091909 (2005).
[4]A. Satta, T. Janssens, T. Clarysse, E. Simoen, M. Meuris, A. Benedetti, I. Hoflijk, B. De Jaeger, C. Demeurisse, and W. Vandervorst, J. Vac. Sci. Technol., B **24**(1), 494 (2006).
[5]G. Thareja, J. Liang, S. Chopra, B. Adams, N. Patil, S. L. Cheng, A. Nainani, E. Tasyurek, Y. Kim, S. Moffatt, R. Brennan, J. McVittie, T.

Kamins, K. Saraswat, and Y. Nishi, presented at the 2010 IEEE International Electron Devices Meeting (unpublished).
[6]R. Duffy, M. Shayesteh, M. White, J. Kearney, and A. M. Kelleher, Appl. Phys. Lett. **96**(23), 231909 (2010).
[7]J. Kim, S. W. Bedell, and D. K. Sadana, Appl. Phys. Lett. **98**(8), 082112 (2011).
[8]J.-H. Park, D. Kuzum, W.-S. Jung, and K. C. Saraswat, IEEE Electron Device Lett. **32**(3), 234 (2011).
[9]G. Dilliway, R. Van Den Boom, A. Moussa, F. Leys, B. Van Daele, B. Parmentier, T. Clarysse, E. R. Simoen, C. Defranoux, M. M. Meuris, A. Benedetti, O. Richard, and H. Bender, ECS Trans. **3**(7), 599 (2006).
[10]D. Cammilleri, F. Fossard, D. Débarre, C. Tran Manh, C. Dubois, E. Bustarret, C. Marcenat, P. Achatz, D. Bouchier, and J. Boulmer, Thin Solid Films **517**(1), 75 (2008).
[11]M. El Kurdi, T. Kociniewski, T. P. Ngo, J. Boulmer, D. Débarre, P. Boucaud, J. F. Damlencourt, O. Kermarrec, and D. Bensahel, Appl. Phys. Lett. **94**(19), 191107 (2009).
[12]H.-Y. Yu, S.-L. Cheng, P. B. Griffin, Y. Nishi, and K. C. Saraswat, IEEE Electron Device Lett. **30**(9), 1002 (2009).
[13]G. Scappucci, G. Capellini, W. C. T. Lee, and M. Y. Simmons, Appl. Phys. Lett. **94**(16), 162106 (2009).
[14]J. M. Hartmann, J. P. Barnes, M. Veillerot, J. M. Fédéli, Q. Benoit, A. La Guillaume, and V. Calvo, J. Cryst. Growth **347**(1), 37 (2012).
[15]R. E. Camacho-Aguilera, Y. Cai, J. T. Bessette, L. C. Kimerling, and J. Michel, Opt. Mater. Express **2**(11), 1462 (2012).
[16]H.-Y. Yu, E. Battal, A. K. Okyay, J. Shim, J.-H. Park, J. W. Baek, and K. C. Saraswat, Curr. Appl. Phys. **13**(6), 1060 (2013).
[17]G. Scappucci, G. Capellini, W. M. Klesse, and M. Y. Simmons, Nanoscale **5**(7), 2600 (2013).
[18]Y. Yamamoto, R. Kurps, C. Mai, I. Costina, J. Murota, and B. Tillack, Solid-State Electron. **83**, 25 (2013).
[19]Y. Moriyama, Y. Kamimuta, Y. Kamata, K. Ikeda, A. Sakai, and T. Tezuka, Appl. Phys. Express **7**(10), 106501 (2014).
[20]P. P. Altermatt, A. Schenk, and G. Heiser, J. Appl. Phys. **100**(11), 113714 (2006).
[21]P. P. Altermatt, A. Schenk, B. Schmithüsen, and G. Heiser, J. Appl. Phys. **100**(11), 113715 (2006).
[22]V. I. Fistul, A. G. Yakovenko, A. A. Gvelesiani, V. N. Tsygankov, and R. L. Krochazhkina, Inorg. Mater. **11**(3), 457 (1975).
[23]M. Koike, Y. Kamata, T. Ino, D. Hagishima, K. Tatsumura, M. Koyama, and A. Nishiyama, J. Appl. Phys. **104**(2), 023523 (2008).
[24]A. V. G. Chizmeshya, C. Ritter, J. Tolle, C. Cook, J. Menendez, and J. Kouvetakis, Chem. Mater. **18**(26), 6266 (2006).
[25]Y. Y. Fang, J. Tolle, A. V. G. Chizmeshya, J. Kouvetakis, V. R. D'Costa, and J. Menendez, Appl. Phys. Lett. **95**(8), 081113 (2009).
[26]J. Xie, J. Tolle, V. R. D'Costa, C. Weng, A. V. G. Chizmeshya, J. Menendez, and J. Kouvetakis, Solid-State Electron. **53**(8), 816 (2009).
[27]J. B. Tice, A. V. G. Chizmeshya, J. Tolle, V. R. D'Costa, J. Menendez, and J. Kouvetakis, Dalton Trans. **39**(19), 4551 (2010).
[28]R. T. Beeler, G. J. Grzybowski, R. Roucka, L. Jiang, J. Mathews, D. J. Smith, J. Menéndez, A. V. G. Chizmeshya, and J. Kouvetakis, Chem. Mater. **23**(20), 4480 (2011).
[29]G. Grzybowski, L. Jiang, J. Mathews, R. Roucka, C. Xu, R. T. Beeler, J. Kouvetakis, and J. Menéndez, Appl. Phys. Lett. **99**(17), 171910 (2011).
[30]C. Xu, R. T. Beeler, L. Jiang, G. Grzybowski, A. V. G. Chizmeshya, J. Menéndez, and J. Kouvetakis, Semicond. Sci. Technol. **28**(10), 105001 (2013).
[31]M. Schubert, *Infrared Ellipsometry on Semiconductor Layer Structures: Phonons, Plasmons, and Polaritons* (Springer, Berlin, Heidelberg, 2004).
[32]H. Fujiwara, *Spectrsocopic Ellipsometry. Principles and Applications* (Wiley, 2007).
[33]G. Dresselhaus, A. Kip, and C. Kittel, Phys. Rev. **98**(2), 368 (1955).
[34]J. Halpern and B. Lax, J. Phys. Chem. Solids **26**(5), 911 (1965).
[35]R. Aggarwal, M. Zuteck, and B. Lax, Phys. Rev. **180**(3), 800 (1969).
[36]D. Rideau, M. Feraille, L. Ciampolini, M. Minondo, C. Tavernier, H. Jaouen, and A. Ghetti, Phys. Rev. B **74**(19), 195208 (2006).
[37]M. El Kurdi, G. Fishman, S. Sauvage, and P. Boucaud, J. Appl. Phys. **107**(1), 013710 (2010).
[38]B. Gelmont and M. S. Shur, J. Appl. Phys. **78**(4), 2846 (1995).
[39]W. G. Spitzer, F. A. Trumbore, and R. A. Logan, J. Appl. Phys. **32**(10), 1822 (1961).
[40]S. S. Li, *Semiconductor Physical Electronics* (Springer, New York, 2006).
[41]M. Oehme, J. Werner, and E. Kasper, J. Cryst. Growth **310**(21), 4531 (2008).
[42]D. B. Cuttriss, Bell Syst. Tech. J. **40**(2), 509 (1961).